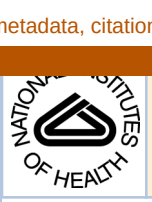

Published in final edited form as:

Eur J Inorg Chem. 2009 November 5; 2009(36): 5506–5515. doi:10.1002/ejic.200900821.

Synthesis, Characterization, and Oxygenation Studies of Carboxylate-Bridged Diiron(II) Complexes with Aromatic Substrates Tethered to Pyridine Ligands and the Formation of a Unique Trinuclear Complex

Simone Friedle and **Stephen J. Lippard***

Department of Chemistry, Massachusetts Institute of Technology, Cambridge, Massachusetts 02139

Abstract

In this study, diiron(II) complexes were synthesized as small molecule mimics of the reduced active sites in the hydroxylase components of bacterial multicomponent monooxygenases (BMMs). Tethered aromatic substrates were introduced in the form of 2-phenoxypyridines, incorporating hydroxy and methoxy functionalities into windmill-type diiron(II) compounds $[Fe_2(\mu\text{-}O_2CAr^R)_2\text{-}(O_2CAr^R)_2(L)_2]$ (**1**–**4**), where $^{-}O_2CAr^R$ is a sterically encumbering carboxylate, 2,6-di(4-fluorophenyl)- or 2,6-di(*p*-tolyl)benzoate (R = 4-FPh or Tol, respectively). The inability of **1**–**4** to hydroxylate the aromatic substrates was ascertained. Upon reaction with dioxygen, compounds **2** and **3** (L = 2-(*m*-MeOPhO)Py, 2-(*p*-MeOPhO)Py, respectively) decompose by a known bimolecular pathway to form mixed-valent diiron(II,III) species at low temperature. Use of 2-(pyridin-2-yloxy)phenol as the ligand L resulted in a doubly-bridged diiron complex (**4**) and an unprecedented phenoxide-bridged triiron(II) complex (**5**) under slightly modified reaction conditions.

Keywords

Diiron hydroxylase synthetic models; oxidation chemistry; sterically hindered carboxylate ligands; X-ray crystallography; EPR spectroscopy

Introduction

Bacterial multicomponent monooxygenases (BMMs) are a class of enzymes that catalyze the regio- and enantioselective oxidation of an array of hydrocarbons, including alkanes, alkenes and aromatics.[1,2] Enzymes belonging to this family include soluble methane monooxygenase (sMMO),[3] toluene/*o*-xylene monooxygenase (ToMO),[4,5] and phenol hydroxylase (PH).[6] The hydroxylase (H) components of these enzymes house a catalytic diiron center, coordinated by four carboxylates from glutamate and two histidine ligands that differ only in the carboxylate binding modes and the ligation of water or hydroxide ion. The diiron active sites of sMMOH in its reduced form and of the manganese(II)-reconstituted ToMOH, an accurate model of its reduced form, are depicted in Figure 1.

The dioxygen activation mechanism of sMMOH has been studied in detail.[3] The reduced state of this enzyme forms a peroxodiiron(III) intermediate ($MMOH_{peroxo}$) in a reaction with dioxygen, which converts to a high-valent diiron(IV) species (Q). The latter is capable of C–

*To whom correspondence should be addressed. lippard@mit.edu.

H bond activation to oxidize methane selectively to methanol. $MMOH_{peroxo}$ also functions as a hydrocarbon oxidant.[7,8] In addition to methane, sMMOH is a competent oxidant for alkynes, amines, and sulfides.[9-13] In ToMOH and PHH, peroxodiiron(III) intermediates are the catalytically relevant species. In contrast to $MMOH_{peroxo}$, these species have featureless UV-vis absorption spectra and significantly different Mössbauer spectroscopic parameters.[14]

Inspired by the versatile oxidation chemistry catalyzed by these non-heme diiron centers, we have been developing synthetic analogues to mimic enzyme function and to gain insight into the complexities of their dioxygen activation mechanisms. The introduction of sterically demanding *m*-terphenyl carboxylates, depicted in Figure 2, has facilitated the synthesis of diiron complexes having the same ligand stoichiometry as that in non-heme diiron enzymes, namely, four carboxylates and two neutral *N*-donors.[15-17] The carboxylate ligands create a protective, hydrophobic sheath around the diiron centers, similar to that in the protein active sites, which prevents them from decomposition and offers excellent solubility in organic solvents. The dinuclear core structures can be tuned by the steric requirements of the carboxylate ligands, which results in doubly- triply-, and quadruply-bridged diiron complexes.[18]

Attempts to oxidize external substrates by oxygenated diiron complexes bearing sterically hindered *m*-terphenyl carboxylates have thus been unsuccessful,[19-21] presumably because the protective bulk around the diiron center blocks substrate access. To circumvent this problem, the substrates were tethered to ancillary neutral donor ligands. With the use of this approach, C–H activation of benzylic moieties in benzyl- and ethylpyridines,[22] oxidation of sulfides and phosphines,[23-25] and oxidative *N*-dealkylation reactions were achieved.[26-29] The extent of oxidation reflected the proximity of the substrate to the diiron center, and little or no oxidation was observed when a substrate moiety was installed in the meta or para position of the pyridine ligand.

Models for ToMOH with polydentate, nitrogen-rich ligands have been reported previously.[30-32] In these studies, aromatic hydroxylation of the ligand was observed, and in one case a peroxodiiron(III) intermediate was characterized.[33] In the present work, we prepared synthetic model complexes for ToMOH and PHH with a carboxylate-rich ligand environment, with aryl groups tethered to the pyridine donor as potential substrates. The *N*-donor ligand 2-(pyridin-2-yloxy)phenol was incorporated to supply phenol, a substrate for PHH. Diiron complexes of this ligand displayed interesting coordination properties, forming dinuclear and trinuclear complexes that were characterized by structural and Mössbauer spectroscopic methods. The dioxygen reactivity of these compounds was investigated by UV-vis spectroscopy and by product analysis.

Results and Discussion

Synthesis and Structural Characterization of $[Fe_2(\mu\text{-}O_2CAr^{4\text{-}FPh})_2(O_2C\text{–}Ar^{4\text{-}FPh})_2(L)_2]$ with L = 2-PhOPy (1), 2-(*m*-Oomph)Py (2), 2-(*p*-Oomph)Py (3)

Reaction of $[Fe_2(\mu\text{-}O_2CAr^{4\text{-}FPh})_2(O_2CAr^{4\text{-}FPh})_2(THF)_2]$ with two equivalents of *N*-donor ligand (L) led to the formation of the diiron(II) complexes **1**, **2**, and **3** having the general formula $[Fe_2(\mu\text{-}O_2CAr^{4\text{-}FPh})_2(O_2CAr^{4\text{-}FPh})_2(L)_2]$ in good yields (Scheme 1).

The structures of **1**–**3** are displayed in Figure 4 and pertinent bond lengths and angles are listed in Table 2. Each compound adopts a windmill geometry[18] in which the iron atoms, related by a center of inversion, are coordinated by two bridging carboxylates, a terminal carboxylate and a nitrogen atom from a pyridine ligand. The geometric parameters of **1**–**3**

are very similar. The rather long Fe–Fe distances lie in a narrow range between 4.368 Å and 4.424 Å and are typical for doubly carboxylate-bridged diiron(II) complexes.[18]

Interestingly, a related diiron(II) compound with 2-phenylthiopyridine, the sulfur analog of 2-phenoxypyridine, adopts a rather different geometry and stoichiometry.[24] In this case, a triply bridged diiron(II) complex forms having a single pyridine donor bound to the diiron unit, the formula being $[Fe_2(\mu\text{-}O_2CAr^{Tol})_3(O_2CAr^{Tol})(L)]$. Figure 3 shows a comparison of this structure with that of **1**. The Fe–S distance in the thioether complex is 3.090 Å, which indicates a very weak interaction between the two atoms made possible by the larger size and more diffuse orbitals of sulfur.[25] In the case of the phenoxypyridine complex, however, no bonding interaction is feasible at an Fe–O distance larger than 3 Å and the complex therefore adopts the typical windmill structure. It is unlikely that the use of different carboxylates, $^{-}O_2CAr^{Tol}$ vs. $^{-}O_2CAr^{4\text{-}FPh}$, would affect the coordination geometry.

Synthesis and Structural Characterization of Compounds 4 and 5 with 2-(Pyridin-2-yloxy)phenol

Treatment of $[Fe_2(\mu\text{-}O_2CAr^{Tol})_2(O_2CAr^{Tol})_2\text{–}(THF)_2]$ with 2-(pyridin-2-yloxy)phenol in CH_2Cl_2 resulted in a lime-green solution, which was initially subjected to vapor diffusion of pentane or Et_2O to isolate the product. We anticipated formation of a doubly bridged diiron complex having a structure analogous to those of compounds **1**–**3**. Colorless block-shaped crystals of the diiron(II) complex $[Fe_2(\mu\text{-}O_2CAr^{Tol})_2(O_2CAr^{Tol})_2(2\text{-}o\text{-}HOPhOPy)_2]$ (**4**) were isolated from the reaction mixture by pentane vapor diffusion in high yield (Scheme 2). Complex **4** has a windmill structure, as occurs in **1**–**3**, with each iron atom being pentacoordinate and an Fe–Fe distance of 4.2743(12) Å. The structure is shown in Figure 5 and selected bond lengths and angles are compared to those of **1**–**3** in Table 2. The tethered phenol forms a strong hydrogen bond to an oxygen atom of a terminal carboxylate, the O–O distance being 2.686(4) Å. This compound is rather air-sensitive and the colorless crystals readily turn black upon exposure to air. An attempt to incorporate meta- and para-(pyridin-2-yloxy)phenol ligands into the diiron(II) complex resulted in the formation colorless crystals, which suffered from loss of solvent and rapid decomposition in air, which precluded their study by X-ray crystallography.

When the reaction mixture from the synthesis of **4**, which contained Et_2O, was further subjected to vapor diffusion of pentane, lime-green crystals of the triiron(II) compound $[Fe_3(\mu\text{-}O_2CAr^{Tol})_2(O_2CAr^{Tol})_2(2\text{-}(o\text{-}\mu\text{-}OPhO)Py)_2]$ (**5**) formed in significant quantity (Scheme 2). Knowing the exact composition of **5** from its crystal structure allowed us to adjust the stoichiometry of reagents to prevent formation of the dinuclear compound **4** as a side product, and the complex could then be prepared in excellent yield (80%). Compound **5** has an unprecedented triiron(II) core, which is displayed in Figure 5. Selected bond lengths and angles are listed in Table 3. Three iron(II) atoms subtend an angle of 134° at the central atom, which resides on a two-fold symmetry axis. The two identical neighboring iron atoms contain a pentacoordinate ligand environment and are each connected to the central atom by a carboxylate and a phenoxide bridge. In contrast to **4**, the phenol is deprotonated, as deduced by charge considerations. The 2-(pyridin-2-yloxy)phenoxide ligand connects all three iron atoms, which gives rise to the bent Fe_3 unit. Space-filling representations in Figure 6 reveal the arrangement of terphenyl units on top and the two pyridine units on the opposite side of the triiron unit. The central iron atom has a four-coordinate, pseudo-tetrahedral environment with only *O*-atom donors, which has not previously been reported for triiron complexes. Other examples of triiron(II) complexes with carboxylate-bridges have been reported previously, but they adopt a linear or nearly linear geometry for the iron atoms.[34-37] The formation of **5** may be driven by the tendency of the phenoxide ligand to

bridge metal ions, as commonly encountered for polynuclear complexes containing phenolic units.[38]

Mössbauer Spectroscopy

Zero-field Mössbauer spectra of **4** and **5** were acquired at 4.2 K and are displayed in Figure 7. For both compounds the Mössbauer isomer shift and quadrupole splitting parameters fall in the ranges δ = 1.17 – 1.23 mm/s and ΔE_Q = 2.91 – 3.08 mm/s, values typical for high-spin diiron(II) complexes.[39-41] The spectra of powdered solid and benzene solution samples of **4** were acquired and fit to a single quadrupole doublet with essentially identical isomer shifts (δ = 1.23(2) and 1.22(2) mm/s) and quadrupole splitting parameters (ΔE_Q = 3.08(2) and 3.07(2) mm/s). The spectra of the solid displayed a somewhat broader linewidth of Γ = 0.38 mm/s (vs. Γ = 0.30 mm/s for the solution sample). These values correspond to those generally observed in carboxylate-rich diiron compounds with an NO_4 coordination environment.[41] This experiment also confirms that the dinuclear complex **4** stays intact in solution and that there is no formation of the trinuclear species **5**. The Mössbauer spectrum of a powdered sample of **5** was fit to a single, rather broad quadrupole doublet with a linewidth of Γ = 0.45(2) mm/s, an isomer shift of δ = 1.18(2) mm/s, and a quadrupole splitting parameter of ΔE_Q = 2.92(2) mm/s (Figure 7B). Despite the significantly different coordination environments of the two different iron sites in this complex - four-coordinate for the central atom and five-coordinate for the outer two iron atoms - their Mössbauer parameters were nearly identical and the two quadrupole doublets could not be resolved. This result is not surprising, considering that the isomer shifts and the quadrupole splitting parameters fall within a narrow range for high spin iron(II) sites.[41] An attempt to deconvolute the overlapping signals by increasing the temperature stepwise from 4.2 K to 200 K did not resolve the spectra. The temperature-dependent Mössbauer parameters of the samples are listed in Table 4. A frozen sample of **5** in a solution of benzene was also measured and, like the solid sample, it revealed only a single, broad quadrupole doublet (Γ = 0.49(2) mm/s) with Mössbauer parameters of δ = 1.24(2) mm/s and ΔE_Q = 2.80(2).

Dioxygen Reactivity Studies

Solutions of **1**–**3** in CH_2Cl_2 were exposed to dioxygen at −78 °C and examined by UV-vis spectroscopy. Broad visible absorption bands at λ_{max} = 700 and 710 nm ($\varepsilon \approx$ 500–600 M^{-1} cm^{-1}) for compounds **2** and **3**, respectively, grew in over 20 min. The spectra (Figure 8) have features nearly identical to those previously reported for oxygenated intermediates of related diiron complexes of *m*-terphenyl carboxylate ligands.[27,42-44] The optical transitions can be assigned to an intervalence charge transfer originating from a mixed-valent tetracarboxylate-bridged diiron(II,III) complex.[42,43] The different electronic properties of the 2-PhOPy pyridine donor ligand vs. those in **2** and **3**, which both contain methoxy-substituted phenoxypyridines, may account for the absence of an absorption band around 700 nm in the reaction of **1** with O_2 at low temperature (Figure 8). EPR spectra of oxygenated solutions of **2**, recorded at 4.2 K, revealed two signals g = 9.1 and g = 2.0, which correspond to a paramagnetic diiron(II,III) species with an S = 9/2 ground state and a diiron(III,IV) species with an S = 1/2 ground state, respectively (Figure 9). Both species are present in significant quantities after 1 min of reaction time, but the diiron(III,IV) species decays and while the amount of diiron(II,III) species increases over the time course of an hour. These two species form in a previously established pathway of intermolecular electron transfer involving an oxygenated high-valent diiron species and the diiron(II) starting material.[45] This bimolecular reaction pathway is frequently observed for the oxygenation of diiron(II) complexes containing the $^{-}O_2CAr^{Tol}$ carboxylate ligand and has been thoroughly investigated by resonance Raman, Mössbauer, UV-vis, EPR spectroscopy, and X-ray crystallography.[29,44-46] The generation of the mixed-valent diiron species depends

on temperature, solvent, and geometry of the diiron(II) complex, but a detailed mechanism has not yet been established.

Solutions of **4** and **5** are remarkably air-sensitive and instantaneously turn deep purple upon exposure to air. When toluene solutions of these complexes were exposed to an excess of dioxygen at low temperature, the absorption spectra (Figure 10) revealed intense phenoxide-to-iron(III) charge-transfer bands at λ_{max} = 515 and 535 nm, respectively, which are characteristic for such compounds.[47,48] The UV-vis spectra of **4** and **5** are identical, displaying an absorption at 385 nm, which can be assigned to an Fe(II) → pyridine charge transfer (MLCT) band.[41] An X-band EPR spectrum of a freeze-quenched oxygenated solution of **4** did not display a characteristic signal for a phenoxyl radical,[49] so this species can be excluded. In general, these radicals are only stable when the ortho and para positions of the phenol ring are blocked.

Phenoxy substituents were appended to the pyridine ligands of the diiron compounds in order to incorporate an aryl group close as a potential substrate for oxygenation. The phenyl linker was chosen to provide additional flexibility and to avoid a benzylic position that is readily oxidized, as previously established for these types of compounds.[22] Methoxy and hydroxy substituents were included to activate the phenyl ring toward electrophilic substitution, because hydroxylation of aromatic substrates occurs by electrophilic attack on the π-system, as observed for peroxo intermediates in sMMOH[7] and ToMOH.[50]

Analysis of the reaction mixture by GC–MS following oxygenation of the diiron(II) complexes **1**–**4**, however, did not reveal oxidation of the *N*-donor ligand. For the oxidation reaction of **3**, the pyridine ligand was recovered quantitatively. The reason for the failed oxidation may be explained by an inherent inability of the intermediate to hydroxylate aromatic substrates. Although benzylic oxidation was achieved in related diiron systems upon oxygenation,[22] the C–H homolytic bond dissociation energy is much larger in aromatic systems (85 kcal/mol vs. ca. 110 kcal/mol, respectively).[51] Alternatively, the substrate moiety may be unfavorably positioned with respect to the peroxodiiron(III) unit. Unlike previous diiron compounds with tethered substrates, the phenyl ring is located farther from the diiron center, as found by X-ray crystallographic structural analysis, and might be sterically unable to approach the oxygenated diiron center.[22-25,29] The oxidation of tethered phosphine and sulfide groups in analogous diiron systems revealed that the extent of oxidation diminishes when the substrate is systematically moved away from the diiron center.[23-25] In order to test this hypothesis, the tethered substrates would need to be redesigned to bring them closer to the diiron center. Alternatively, a diiron complex with less bulky carboxylates could be used to reduce steric crowding at the dimetallic center.

Conclusions

The palette of carboxylate-rich diiron(II) compounds with tethered substrates was expanded in this work. Previously, oxidation of sulfide, phosphine, and benzyl-moieties and oxidative *N*-dealkylation were established with these systems. A series of doubly bridged diiron(II) complexes were prepared with methoxy- and hydroxy-substituted phenoxypyridine ligands to serve as substrates for aromatic hydroxylation following the introduction of dioxygen. In the reaction of these diiron(II) complexes with dioxygen no oxidation of the aryl substituent was observed, indicating the importance of substrate proximity to the diiron active site. Interesting coordination chemistry was observed with the 2-(pyridin-2-yloxy)phenol ligand that led to the formation of two complexes of different nuclearity. In one case, the hydroxyl group on the phenoxypyridine is protonated and a diiron(II) complex is formed. Upon deprotonation, the phenoxide bridges two iron centers and an unprecedented triiron(II) core structure was obtained.

Experimental Section

General Procedures and Methods

Tetrahydrofuran (THF), diethylether (Et_2O), pentane, and dichloromethane (CH_2Cl_2) were saturated with nitrogen and purified by passage through activated alumina columns under an argon atmosphere. Dry 1,2-dichloroethane (DCE) was purchased from Aldrich. Dioxygen (99.994%, BOC gases) was dried by passing the gas stream through a column of Drierite®. The synthesis and characterization of compounds $[Fe_2(\mu\text{-}O_2CAr^{4\text{-}FPh})_2(O_2CAr^{4\text{-}FPh})_2(THF)_2]$[18] and $[Fe_2(\mu\text{-}O_2CAr^{Tol})_2(O_2CAr^{Tol})_2(THF)_2]$[15] are reported elsewhere. The ligands 2-(3-methoxyphenoxy)pyridine [2-(*m*-MeOPhO)Py], 2-(4-methoxyphenoxy)pyridine [(2-(*p*-MeOPhO)Py], and 2-(pyridin-2-yloxy)phenol [2-(*o*-HOPhO)Py] were prepared using modified literature procedures.[52] All other reagents were obtained from commercial sources and used as received. Air sensitive manipulations were performed using Schlenk techniques or under nitrogen atmosphere in an MBraun glovebox.

Physical measurements

FT-IR spectra were recorded on a Thermo Nicolet Avatar 360 spectrometer with OMNIC software. Melting points were acquired on an electrothermal Mel-Temp melting point apparatus. All gas chromatographic studies were carried out on an Agilent 6890 gas chromatograph attached to an Agilent 5973N mass selective detector. An HP-5ms (5%-phenyl-substituted methylpolysiloxane) capillary column (30 m × 0.25 mm × 0.25 μm) was used.

$[Fe_2(\mu\text{-}O_2CAr^{4\text{-}FPh})_2(O_2CAr^{4\text{-}FPh})_2(2\text{-}PhOPy)_2]$ (1)

A pale yellow solution of $[Fe_2(\mu\text{-}O_2CAr^{4\text{-}FPh})_2(O_2CAr^{4\text{-}FPh})_2(THF)_2]$ (90.0 mg, 60.3 μmol) in CH_2Cl_2 (3 mL) was combined with 2-phenoxypyridine (2-PhOpy; 20.7 mg, 121 μmol) and allowed to react for 10 min. Vapor diffusion of Et_2O into the filtered solution resulted in the formation of pale yellow crystals of **1** suitable for X-ray crystallography. Yield: 43.0 mg (41%). FT-IR (KBr, cm^{-1}): 3106 (w), 3065 (w), 3035 (w), 2961 (w), 2846 (w), 1605 (s), 1569 (m), 1534 (m), 1511 (vs), 1489 (m), 1473 (s), 1454 (s), 1439 (s), 1410 (m), 1383 (m), 1281 (m), 1226 (s), 1204 (m),1159 (s), 1096 (m), 1014 (m), 892 (w), 859 (m), 845 (m), 839 (m), 807 (m), 789 (m), 774 (m), 752 (w), 733 (w), 712 (w). 691 (w), 579 (w), 555 (m), 528 (m), 478 (w), 460 (w). Anal. Calcd. for **1**, $Fe_2F_8O_{10}N_2C_{98}H_{62}$: C, 69.60; H, 3.70; N, 1.66. Found: C, 69.23; H, 3.83; N, 1.35. Mp: 163–165 °C (dec).

$[Fe_2(\mu\text{-}O_2CAr^{4\text{-}FPh})_2(O_2CAr^{4\text{-}FPh})_2(2\text{-}(m\text{-}MeOPhO)Py)_2]$ (2)

A solution of 2-(*m*-MeOPhO)py (32.3 mg, 161 μmol) was added to a stirred suspension of $[Fe_2(\mu\text{-}O_2CAr^{4\text{-}FPh})_2(O_2CAr^{4\text{-}FPh})_2(THF)_2]$ (120 mg, 80.4 μmol) in 5 mL of CH_2Cl_2 and allowed to react for 10 min. After the yellow solution had been filtered, it was subjected to Et_2O vapor diffusion to yield pale yellow-green blocks of **2** suitable for X-ray crystallography. Yield: 94.5 mg (70%). FT-IR (KBr, cm^{-1}): 3057 (w), 2961 (w), 2921 (w), 2851 (w), 1605 (s), 1573 (m), 1455 (m), 1437 (m), 1411 (m), 1262 (m), 1160 (m), 1142 (m), 1040 (m), 1017 (m), 853 (w), 80 (m), 788 (w), 770 (w), 712 (m), 555 (w). Anal. Calcd. for **2**·0.25CH_2Cl_2, $Fe_2F_8O_{12}N_2C_{100.25}H_{66.5}Cl_{0.5}$: C, 67.93; H, 3.78; N, 1.58. Found: C, 67.90; H, 3.88; N, 1.13. Mp: 158–160 °C (dec).

$[Fe_2(\mu\text{-}O_2CAr^{4\text{-}FPh})_2(O_2CAr^{4\text{-}FPh})_2(2\text{-}(p\text{-}MeOPhO)Py)_2]$ (3)

Pale yellow-green X-ray quality crystals of **3** formed by vapor diffusion of pentanes into a reaction mixture of $[Fe_2(\mu\text{-}O_2CAr^{4\text{-}FPh})_2(O_2CAr^{4\text{-}FPh})_2(THF)_2]$ (120 mg, 80.4 μmol) and 2-(*p*-MeOPhO)py (32.3 mg, 161 μmol) in 5 mL of CH_2Cl_2. Yield: 118 mg (83%). FT-IR (KBr, cm^{-1}): 3065 (w), 2952 (w), 2837 (w), 1604 (s), 1547 (m), 1511 (s), 1473 (m), 1438

(m), 1277 (w), 1244 (m), 1222 (m), 1200 (m), 1160 (m), 1060 (w), 1016 (w), 846 (m), 809 (m), 793 (w), 775 (w), 735 (w), 713 (w), 550 (w). Anal. Calcd. for **3**, $Fe_2F_8O_{12}N_2C_{100}H_{66}$: C, 68.58; H, 3.80; N, 1.60. Found: C, 68.85; H, 3.95; N, 1.95. Mp: 165–167 °C (dec).

$[Fe_2(\mu\text{-}O_2CAr^{Tol})_2(O_2CAr^{Tol})_2(2\text{-}(o\text{-}HOPhO)Py)_2]$ (4)

A pale yellow CH_2Cl_2 solution of $[Fe_2(\mu\text{-}O_2CAr^{Tol})_2(O_2CAr^{Tol})_2(THF)_2]$ (50 mg, 34 μmol) was combined with a solution of 2-(o-HOPhO)Py (13 mg, 70 μmol) and allowed to react for 10 min. Vapor diffusion of pentane into the lime-green filtered solution (total volume 2 mL) resulted in the formation of colorless crystals of **4** suitable for X-ray crystallography. Yield: 49 mg (86%). FT-IR (KBr, cm^{-1}): 3050 (w), 3019 (w), 2917 (w), 2857 (w), 1605 (s), 1590 (s), 1574 (s), 1563 (s), 1515 (m), 1492 (m), 1472 (s), 1455 (m), 1437 (s), 1411 (m), 1378 (m), 1277 (s), 1253 (w), 1185 (w), 1148 (w), 1108 (w), 1094 (w), 1016 (w), 897 (w), 861 (w), 817 (w), 800 (m), 767 (m), 734 (m), 712 (w), 702 (w), 584 (w), 545 (w), 519 (w), 452 (w). Anal. Calcd. for **4**, $Fe_2O_{12}N_2C_{106}H_{86}$: C, 75.27; H, 5.12; N, 1.66. Found: C, 74.75; H, 5.10; N, 1.93. Mp: 118–120 °C (dec).

$[Fe_3(\mu_2\text{-}O_2CAr^{Tol})_2(O_2CAr^{Tol})_2(2\text{-}(o\text{-}\mu_2\text{-}O\text{-}PhO)Py)_2]$ (5)

In a procedure similar to that described above, a CH_2Cl_2 solution of $[Fe_2(\mu\text{-}O_2CAr^{Tol})_2(O_2CAr^{Tol})_2(THF)_2]$ (47 mg, 32 μmol) was combined with a solution of 2-(o-HOPhO)Py (8.0 mg, 43 μmol). The total volume of the resulting solution was ca. 2.5 mL. After filtration of the solution, ca. 2 mL of Et_2O was added and the lime-green solution was subjected to vapor diffusion of pentane. Lime-green blocks of **5**, suitable for X-ray crystallography, were harvested. Yield: 28 mg (80%). FT-IR (KBr, cm^{-1}): 3054 (w), 3021 (w), 2916 (w), 2854 (w), 1604 (m), 1597 (m), 1572 (m), 1545 (s), 1514 (s), 1490 (s), 1472 (s), 1436 (s), 1411 (m), 1387 (s), 1286 (s), 1257 (s), 1181 (w), 1156 (w), 1110 (w), 1098 (w), 1022 (w), 898 (w), 859 (w), 834 (w), 817 (m), 800 (m), 785 (m), 768 (m), 753 (m), 738 (m), 715 (m), 699 (w), 582 (m), 552 (w), 527 (m), 455 (w), 425 (w). Anal. Calcd. for **5**, $Fe_3O_{12}N_2C_{106}H_{84}$: C, 72.94; H, 4.85; N, 1.61. Found: C, 72.89; H, 4.98; N, 1.59. Mp: 215–217 °C (dec).

X-ray Crystallographic Studies

Single crystals were taken directly from the reaction vessel, coated with Paratone-N oil, and mounted at room temperature on the tips of quartz fibers or nylon loops (OXFORD magnetic mounting system), and cooled to 110 K under a stream of cold N_2 maintained by a KRYO-FLEX low-temperature apparatus. Intensity data were collected on a Bruker (formerly Siemens) APEX CCD diffractometer with graphite-monochromated Mo Kα radiation (λ = 0.71073 Å) controlled by a Pentium-based PC running the SMART software package.[53] The structures were solved by direct methods and refined on F^2 by using the SHELXTL-97 software.[54,55] Empirical absorption corrections were applied with SADABS[56] and the structures were checked for higher symmetry with PLATON.[57] All non-hydrogen atoms were refined anisotropically. Hydrogen atoms were generally assigned idealized positions and given thermal parameters equivalent to either 1.5 (methyl hydrogen atoms) or 1.2 (all other hydrogen atoms) times the thermal parameter of the carbon to which they were attached. The hydrogen atom of the hydroxyl group (O5) of the 2-(pyridin-2-yloxy)phenol ligand in **4** was located on a difference electron density map. Complex **1** crystallizes without any solvent in the lattice. A pentane and a CH_2Cl_2 molecule share one position with a refined ratio of 73:27 in compound **2**. A molecule of CH_2Cl_2 was identified in the asymmetric unit of complex **3**. In the structure of **4**, a pentane molecule was disordered over two positions with 58% and 42% occupancy. Complex **5** contains two molecules of CH_2Cl_2 per triiron unit. Crystal data, data collection parameters, and structure refinement details for **1**–**5** are provided in Table 1. The files CCDC 744098–744102 contain crystallographic information for **1**–**5**, respectively, which can be obtained free of charge

from The Cambridge Crystallographic Data Centre at www.ccdc.cam.ac.uk./data_request/cif.

Mössbauer Spectroscopy

Mössbauer spectra were obtained on an MS1 spectrometer (WEB Research Co.) with a ^{57}Co source in a Rh matrix maintained at room temperature. All samples were enriched with ^{57}Fe (40%) and prepared from $^{57}Fe(OTf)_2{\cdot}2MeCN$, which was synthesized following a published procedure.[58] Solid samples of **4** and **5** were prepared by suspending ca. 15 mg of pulverized compound in Apiezon N-grease and loading the suspension into a nylon sample holder. Solution samples of **4** and **5** were prepared in benzene and frozen. Data were acquired at temperatures ranging from 4.2 K to 200 K. The isomer shift (δ) values are reported with respect to natural iron foil that was used for velocity calibration at room temperature. The spectra were fit to Lorentzian lines by using the WMOSS plot and fit software.[59]

Oxidation Reactions

Solutions of **1**–**4** in CH_2Cl_2 prepared under anaerobic conditions in a glove box and dry dioxygen was bubbled through these solutions for at least 2–4 min at −78 °C. The reaction mixture was allowed to warm up to 25 °C and stirred overnight. For the analysis of the products from the oxidation reaction, it was necessary to remove iron from the solutions. A chelating resin, CHELEX-100®, was employed for this purpose. The resulting pale-colored solutions were filtered and analyzed by GC-MS spectrometry by comparing their properties to those of authentic samples.

UV-vis Spectroscopy Studies

UV-vis spectra were recorded on a Hewlett-Packard 8453 diode array spectrophotometer. Solutions of [Fe_2] in CH_2Cl_2 or toluene under N_2-atmosphere were cooled to −78 °C (acetone/dry ice) in a custom-made quartz-cuvette, 1 cm pathlength, fused into a vacuum-jacketed dewar. Dry O_2 was bubbled through the solutions for 30 s, and UV-vis spectra were recorded at various time intervals.

EPR Spectroscopy

X-band EPR spectra were acquired on a Bruker EMX EPR spectrometer at the Department of Chemistry Instrumentation Facilities at MIT running Bruker Win-EPR software. An OXFORD instruments EPR 900 cryostat and an ITC503 controller were used to maintain the temperature at 4 K. Samples were prepared by transferring 300 μL aliquots of a 3.0 M solution of **3** in CH_2Cl_2 into EPR tubes under anaerobic conditions, which were then septum-sealed. Dry dioxygen was bubbled through these solutions for at least 20 s at −78 °C. The oxygenated solutions were frozen after 1, 2, 5, and 60 min reaction time at 77 K.

Acknowledgments

This work was supported by Grant GM032134 from the National Institute of General Medical Sciences. We thank Dr. Sebastian Stoian for assistance in acquiring the Mössbauer spectra and Dr. Erwin Reisner for helpful discussions.

References

1. Sazinsky MH, Lippard SJ. Acc Chem Res. 2006; 39:558–566. [PubMed: 16906752]
2. Murray LJ, Lippard SJ. Acc Chem Res. 2007; 40:466–474. [PubMed: 17518435]
3. Merkx M, Kopp DA, Sazinsky MH, Blazyk JL, Müller J, Lippard SJ. Angew Chem, Int Ed. 2001; 40:2782–2807.

4. Sazinsky MH, Bard J, Di Donato A, Lippard SJ. J Biol Chem. 2004; 279:30600–30610. [PubMed: 15096510]
5. McCormick MS, Sazinsky MH, Condon KL, Lippard SJ. J Am Chem Soc. 2006; 128:15108–15110. [PubMed: 17117860]
6. Sazinsky MH, Dunten PW, McCormick MS, Di Donato A, Lippard SJ. Biochemistry. 2006; 45:15392–15404. [PubMed: 17176061]
7. Beauvais LG, Lippard SJ. J Am Chem Soc. 2005; 127:7370–7378. [PubMed: 15898785]
8. Valentine AM, Stahl SS, Lippard SJ. J Am Chem Soc. 1999; 121:3876–3887.
9. Colby J, Stirling DI, Dalton H. Biochem J. 1977; 165:395–402. [PubMed: 411486]
10. Prior SD, Dalton H. FEMS Microbiol Lett. 1985; 29:105–109.
11. Green J, Dalton H. J Biol Chem. 1989; 264:17698–17703. [PubMed: 2808342]
12. Fox BG, Borneman JG, Wackett LP, Lipscomb JD. Biochemistry. 1990; 29:6419–6427. [PubMed: 2207083]
13. Fuse H, Ohta M, Takimura O, Murakami K, Inoue J, Yamaoka Y, Oclarit JM, Omori T. Biosci Biotech Biochem. 1998; 62:1925–1931.
14. Murray LJ, García-Serres R, Naik S, Huynh BH, Lippard SJ. J Am Chem Soc. 2006; 128:7458–7459. [PubMed: 16756297]
15. Lee DW, Lippard SJ. J Am Chem Soc. 1998; 120:12153–12154.
16. Hagadorn JR, Que L Jr, Tolman WB. J Am Chem Soc. 1998; 120:13531–13532.
17. Tolman WB, Que L Jr. J Chem Soc, Dalton Trans. 2002; 5:653–660.
18. Lee D, Lippard SJ. Inorg Chem. 2002; 41:2704–2719. [PubMed: 12005495]
19. Que L, Tolman WB. Nature. 2008; 455:333–340. [PubMed: 18800132]
20. Costas M, Chen K, Que L. Coord Chem Rev. 2000; 200-202:517–544.
21. Feig AL, Lippard SJ. Chem Rev. 1994; 94:759–805.
22. Carson EC, Lippard SJ. Inorg Chem. 2006; 45:828–836. [PubMed: 16411721]
23. Carson EC, Lippard SJ. J Am Chem Soc. 2004; 126:3412–3413. [PubMed: 15025454]
24. Carson EC, Lippard SJ. Inorg Chem. 2006; 45:837–848. [PubMed: 16411722]
25. Reisner E, Abikoff TC, Lippard SJ. Inorg Chem. 2007; 46:10229–10240. [PubMed: 17973373]
26. Lee D, Lippard SJ. J Am Chem Soc. 2001; 123:4611–4612. [PubMed: 11457252]
27. Yoon SH, Lippard SJ. Inorg Chem. 2003; 42:8606–8608. [PubMed: 14686832]
28. Yoon S, Lippard SJ. Inorg Chem. 2006; 45:5438–5446. [PubMed: 16813407]
29. Carson EC, Lippard SJ. J Inorg Biochem. 2006; 100:1109–1117. [PubMed: 16439023]
30. Furutachi H, Murayama M, Shiohara A, Yamazaki S, Fujinami S, Uehara A, Suzuki M, Ogo S, Watanabe Y, Maeda Y. Chem Commun. 2003:1900–1901.
31. Avenier F, Dubois L, Latour J-M. New J Chem. 2004; 28:782–784.
32. Menage S, Galey J-B, Dumats J, Hussler G, Seite M, Luneau IG, Chottard G, Fontecave M. J Am Chem Soc. 1998; 120:13370–13382.
33. Yamashita M, Furutachi H, Tosha T, Fujinami S, Saito W, Maeda Y, Takahashi K, Tanaka K, Kitagawa T, Suzuki M. J Am Chem Soc. 2007; 129:2–3. [PubMed: 17199259]
34. Rardin RL, Bino A, Poganiuch P, Tolman WB, Liu S, Lippard SJ. Angew Chem, Int Ed. 1990; 29:812–814.
35. Rardin RL, Poganiuch P, Bino A, Goldberg DP, Tolman WB, Liu S, Lippard SJ. J Am Chem Soc. 1992; 114:5240–5249.
36. Reynolds RA III, Dunham WR, Coucouvanis D. Inorg Chem. 1998; 37:1232–1241. [PubMed: 11670328]
37. Reisner E, Telser J, Lippard SJ. Inorg Chem. 2007; 46:10754–10770. [PubMed: 17997551]
38. Ambrosi G, Formica M, Fusi V, Giorgi L, Micheloni M. Coord Chem Rev. 2008; 252:1121–1152.
39. Gütlich, P.; Ensling, J. Inorganic Electronic Structure and Spectroscopy. Solomon, EI.; Lever, ABP., editors. Vol. I. Wiley & Sons; New York: 1999. p. 161-211.
40. Münck, E. Physical Methods in Bioinorganic Chemistry: Spectroscopy and Magnetism. Que, L., Jr, editor. University Science Books; Sausalito, CA: 2000. p. 287-319.

41. Yoon S, Lippard SJ. J Am Chem Soc. 2005; 127:8386–8397. [PubMed: 15941272]
42. Lee D, Krebs C, Huynh BH, Hendrich MP, Lippard SJ. J Am Chem Soc. 2000; 122:5000–5001.
43. Lee D, DuBois JL, Pierce B, Hedman B, Hodgson KO, Hendrich MP, Lippard SJ. Inorg Chem. 2002; 41:3172–3182. [PubMed: 12054996]
44. Carson, EC. Doctoral Dissertation in Inorganic Chemistry. Vol. Chapter 4. Massachusetts Institute of Technology; Cambridge, MA: 2005.
45. Lee D, Pierce B, Krebs C, Hendrich MP, Huynh BH, Lippard SJ. J Am Chem Soc. 2002; 124:3993–4007. [PubMed: 11942838]
46. Lee D, Du Bois J, Petasis D, Hendrich MP, Krebs C, Huynh BH, Lippard SJ. J Am Chem Soc. 1999; 121:9893–9894.
47. Gaber BP, Miskowski V, Spiro TG. J Am Chem Soc. 1974; 96:6868–6873. [PubMed: 4436502]
48. Koch SA, Millar M. J Am Chem Soc. 1982; 104:5255–5257.
49. Altwicker ER. Chem Rev. 1967; 67:475–531.
50. Murray LJ, Naik SG, Ortillo DO, García-Serres R, Lee JK, Huynh BH, Lippard SJ. J Am Chem Soc. 2007; 129:14500–14510. [PubMed: 17967027]
51. Wade, LG. Organic Chemistry. 4. Prentice Hall; Upper Saddle River, New Jersey: 1998.
52. Hill AJ, McGraw WJ. J Org Chem. 1949; 14:783–788.
53. SMART, Software for the CCD Detector System, version 5.6. Bruker AXS; Madison, WI: 2000.
54. Sheldrick GM. Acta Crystallogr, Sect A. 2008; A64:112–122. [PubMed: 18156677]
55. Sheldrick, GM. SHELXTL-97. University of Göttingen; Göttingen, Germany: 2000.
56. Sheldrick, GM. SADABS: Area-Detector Absorption Correction. University of Göttingen; Göttingen, Germany: 2001.
57. Spek, AL. PLATON, A Multipurpose Crystallographic Tool. Utrecht University; Utrecht, The Netherlands: 2000.
58. Hagen KS. Inorg Chem. 2000; 39:5867–5869. [PubMed: 11151391]
59. Kent, TA. WMOSS; Mössbauer Spectral Analysis Software, version 2.5. Minneapolis: 1998.

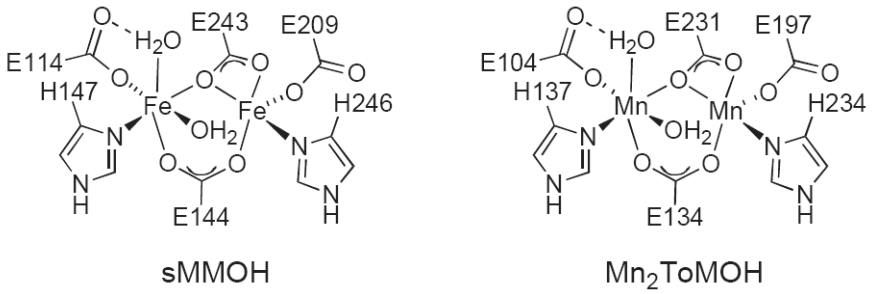

Figure 1.
Structural diagrams of the diiron(II) active site in reduced sMMOH and a dimanganese analog of the reduced diiron(II) center in ToMOH.

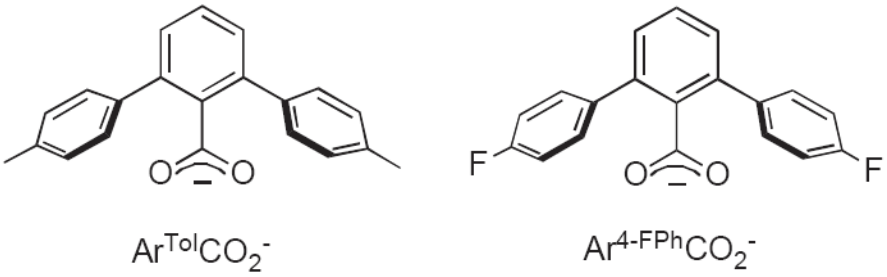

Figure 2.
Sterically demanding terphenylcarboxylate ligands used in these studies.

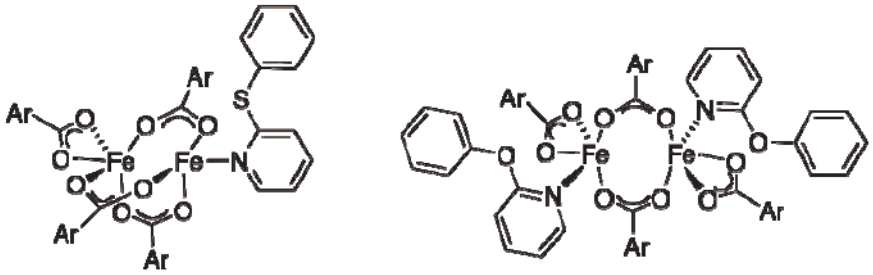

Figure 3.
Comparison of the structures of $[Fe_2(\mu\text{-}O_2CAr^{Tol})_3(O_2CAr^{Tol})(2\text{-PhSPy})]$[24] (left) and $[Fe_2(\mu\text{-}O_2CAr^{4\text{-}FPh})_2(O_2CAr^{4\text{-}FPh})_2(2\text{-PhOPy})_2]$ (**1**; right).

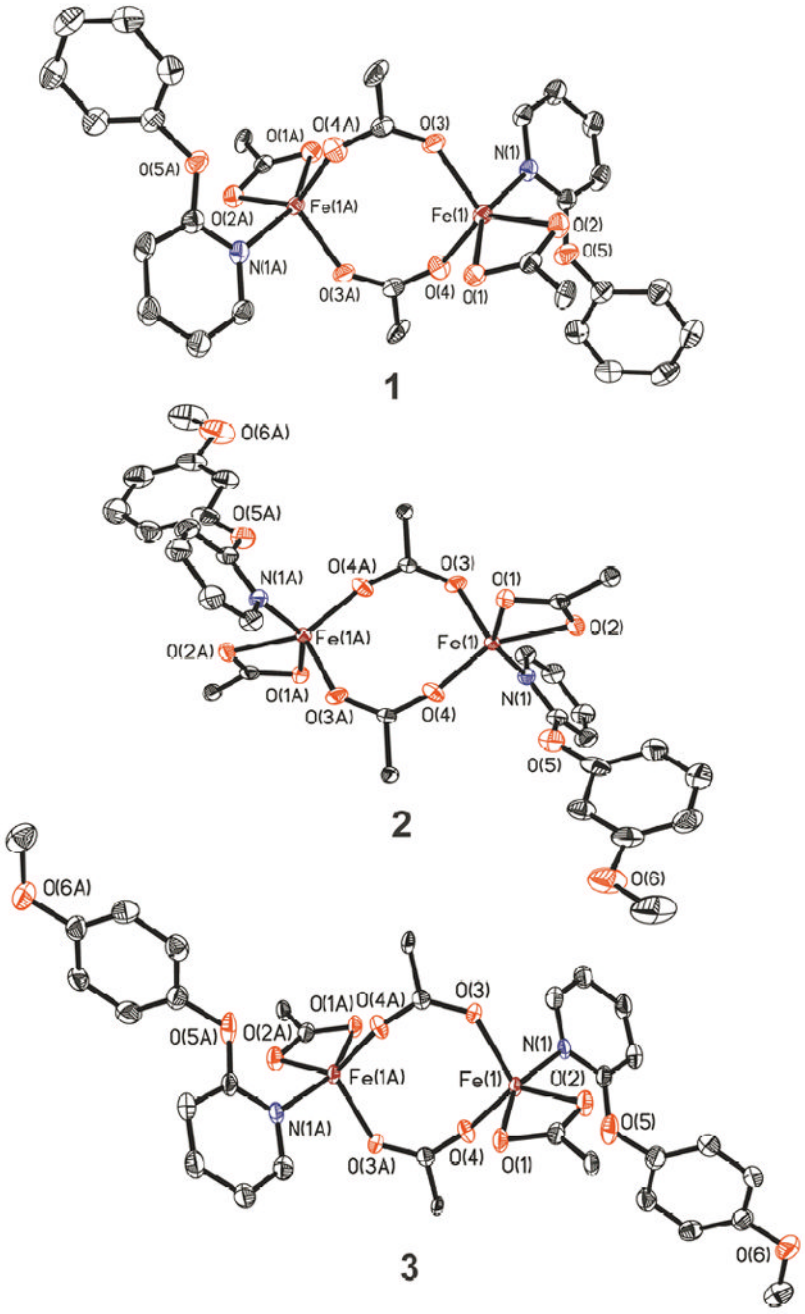

Figure 4.

ORTEP diagrams of $[Fe_2(\mu\text{-}O_2CAr^{4\text{-}FPh})_2(O_2CAr^{4\text{-}FPh})_2(2\text{-}PhOPy)_2]$ (**1**), $[Fe_2(\mu\text{-}O_2CAr^{4\text{-}FPh})_2(O_2CAr^{4\text{-}FPh})_2(2\text{-}(m\text{-}MeOPhO)Py)_2]$ (**2**), and $[Fe_2(\mu\text{-}O_2CAr^{4\text{-}FPh})_2(O_2CAr^{4\text{-}FPh})_2(2\text{-}(p\text{-}MeOPhO)Py)_2]$ (**3**) showing 50% probability thermal ellipsoids for all non-hydrogen atoms. The 4-fluorophenyl groups of the $^{-}O_2CAr^{4\text{-}FPh}$ ligands are omitted for clarity.

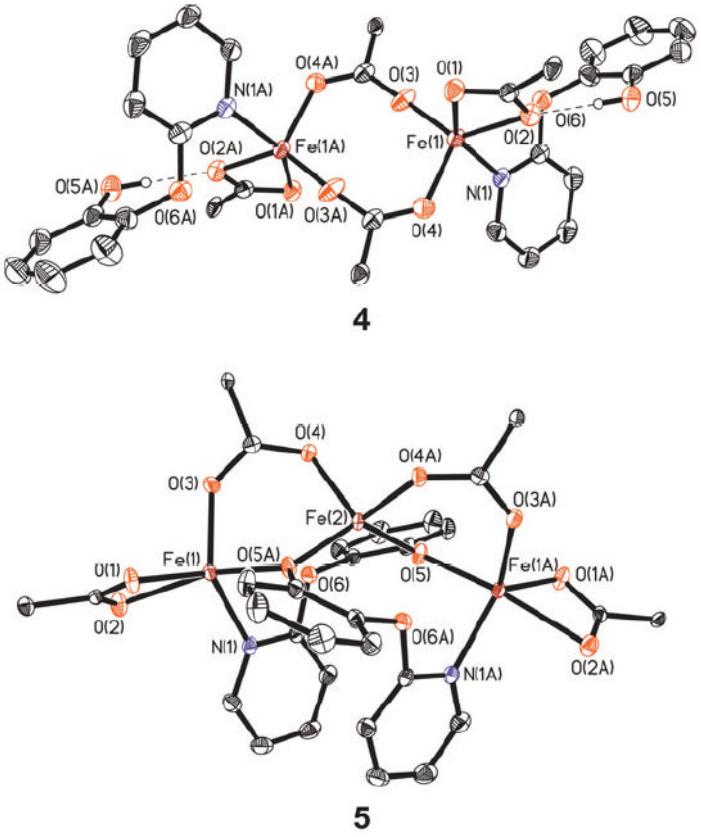

Figure 5.

ORTEP diagrams of $[Fe_2(\mu\text{-}O_2CAr^{Tol})_2(O_2CAr^{Tol})_2(2\text{-}(o\text{-}HOPhO)Py)_2]$ (**4**) and $[Fe_3(\mu_2\text{-}O_2CAr^{Tol})_2(O_2CAr^{Tol})_2(2\text{-}(o\text{-}\mu_2\text{-}O\text{-}PhO)Py)_2]$ (**5**), showing 50% probability thermal ellipsoids for all non-hydrogen atoms. The tolyl groups of the $^{-}O_2CAr^{Tol}$ ligands are omitted for clarity.

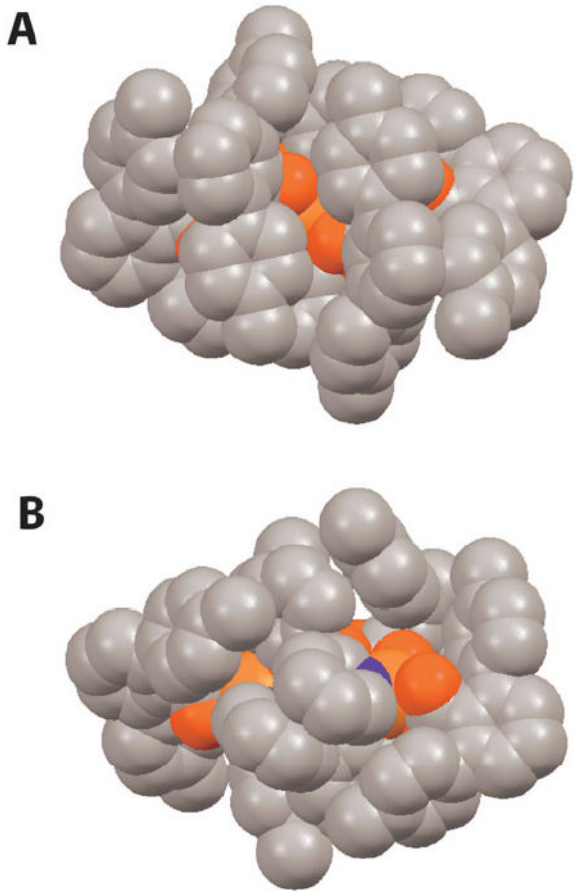

Figure 6.
Space-filling representation of $[Fe_3(\mu_2\text{-}O_2CAr^{Tol})_2(O_2CAr^{Tol})_2(2\text{-}(o\text{-}\mu_2\text{-}O\text{-}PhO)Py)_2]$ (**5**), displaying views with respect to the triiron vector from the top (A) and from the bottom (B), where N is colored blue, O red, and Fe orange. Hydrogen atoms are omitted.

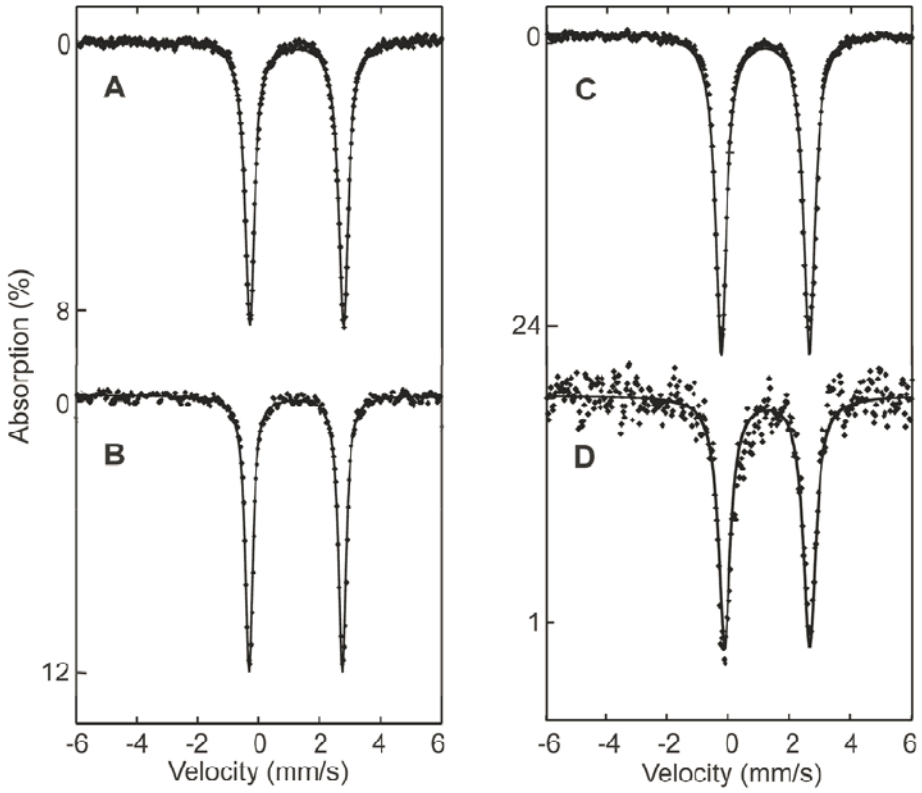

Figure 7.
Zero-field Mössbauer spectra [experimental data (◆), calculated fit (–)] of solid samples of **4** (A) and **5** (C) and solution samples of **4** (B) and **5** (D) in benzene. All samples were recorded at 4.2 K, except sample D, which was acquired at 90 K.

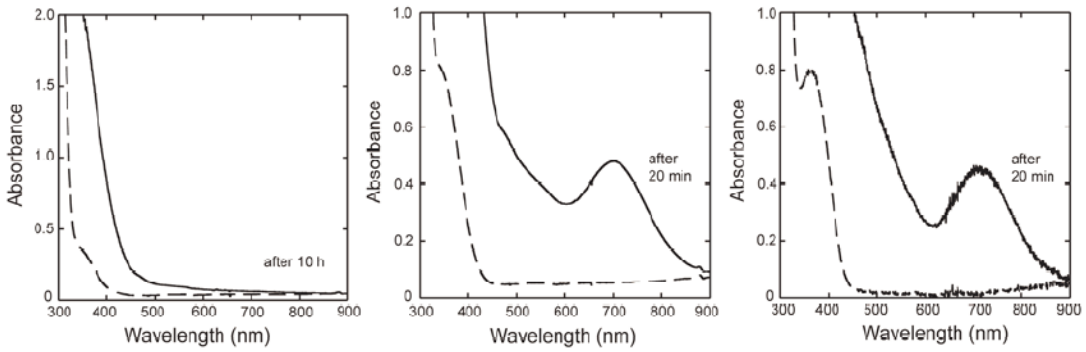

Figure 8.

UV-vis spectra of O_2 reactions, recorded at –78 °C in CH_2Cl_2, of $[Fe_2(\mu\text{-}O_2CAr^{4\text{-}FPh})_2(O_2CAr^{4\text{-}FPh})_2(2\text{-}PhOPy)_2]$ (**1**, left), $[Fe_2(\mu\text{-}O_2CAr^{4\text{-}FPh})_2(O_2CAr^{4\text{-}FPh})_2(2\text{-}(m\text{-}OMePhO)Py)_2]$ (**2**, center), and $[Fe_2(\mu\text{-}O_2CAr^{4\text{-}FPh})_2(O_2CAr^{4\text{-}FPh})_2(2\text{-}(p\text{-}OMePhO)Py)_2]$ (**3**, right), displaying the spectra of the diiron(II) compound (---) and the intermediates (—).

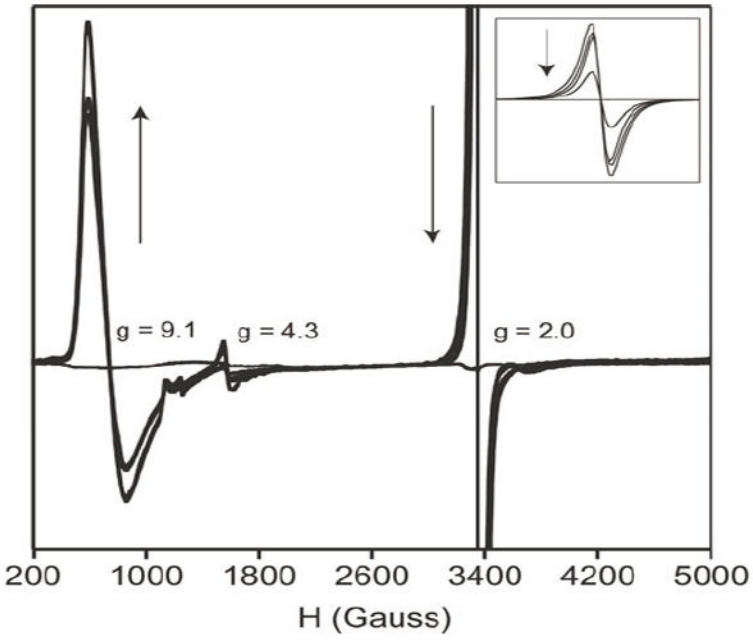

Figure 9.
X-band EPR spectra of frozen solution samples of **2** and oxygenated **2** recorded at 4 K. The spectra represent 1, 2, 5, and 60 min reactions of **2** with dioxygen at −78 °C. The inset displays the decay of the signal at g = 2.0. The signal at g = 4.3 arises from a small amount of high-spin Fe(III) impurity.

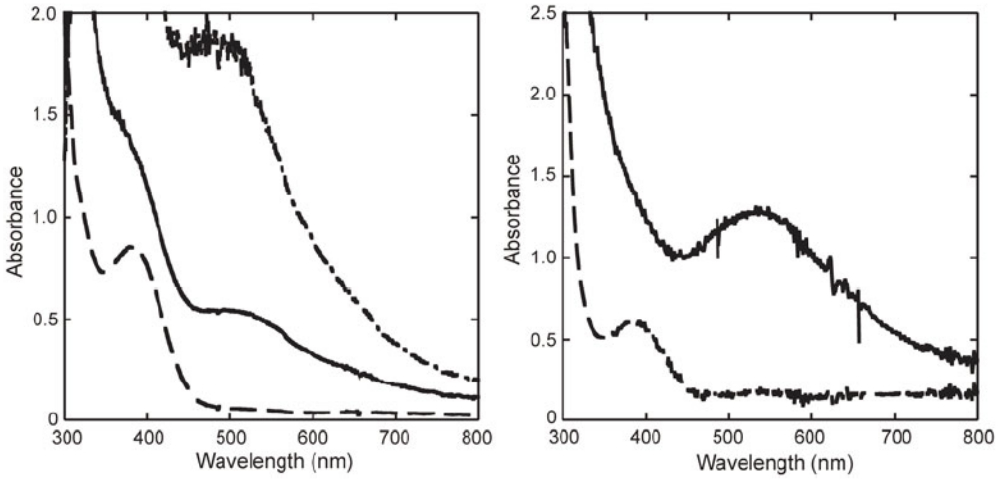

Figure 10.

UV-vis spectra of O_2 reactions, recorded at −78 °C in toluene. Left: [$Fe_3(\mu_2$-$O_2CAr^{Tol})_2(O_2CAr^{Tol})_2$(2-($o$-$\mu_2$-O-PhO)Py)$_2$] (**5**) (---); the intermediate after 30 min (—) and after 7 h (–●–). Right: [$Fe_2(\mu$-$O_2CAr^{4\text{-FPh}})_2(O_2CAr^{4\text{-FPh}})_2$(2-PhOPy)$_2$] (**4**) (---), the intermediate (—) after 3 h.

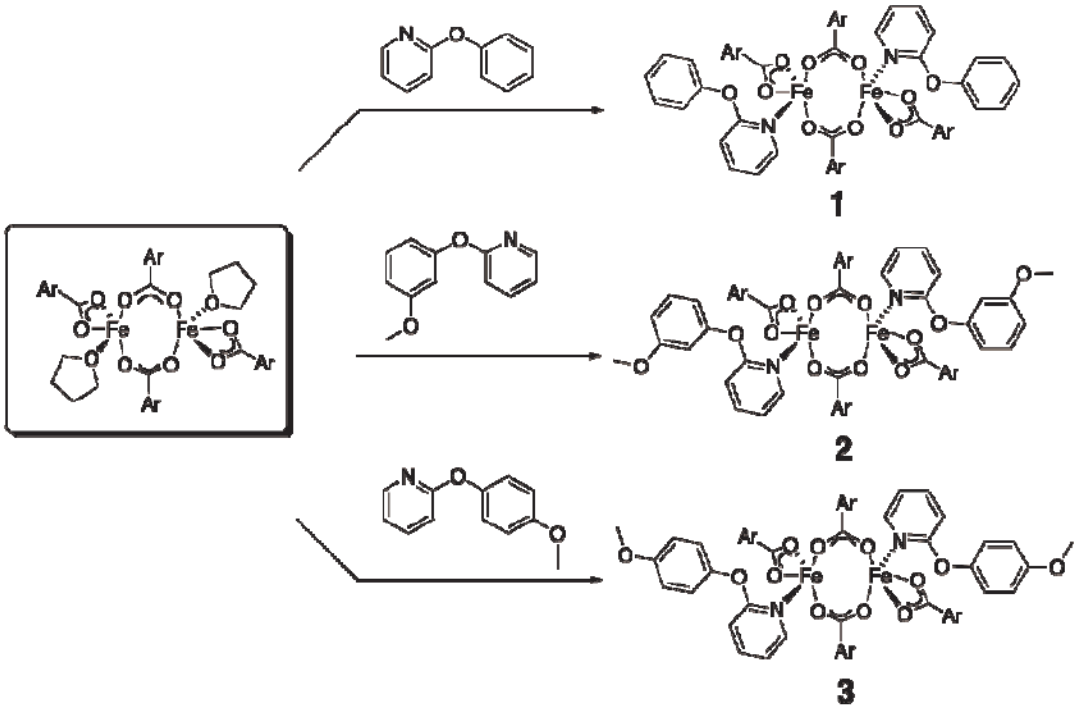

Scheme 1.

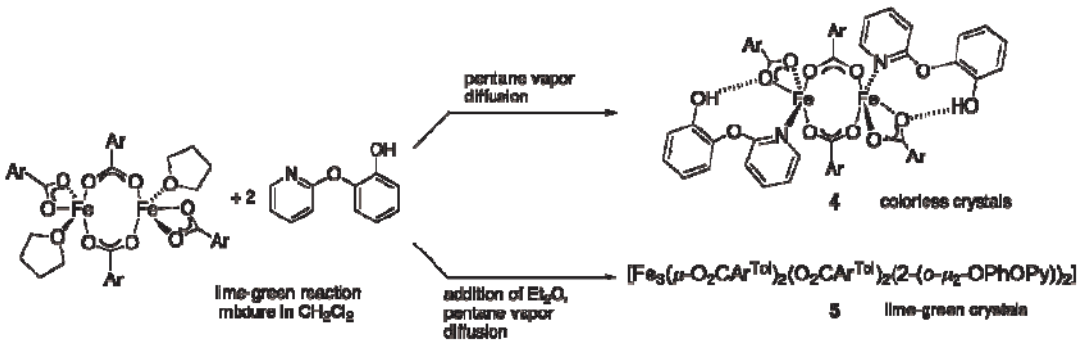

Scheme 2.

Table 1

Crystal Data and Details of Data Collection for **1**–**5**.

	1	**2·1.5C_5H_{12}·0.5CH_2Cl_2**	**3·2CH_2Cl_2**	**4·C_5H_{12}**	**5·2CH_2Cl_2**
Empirical formula	$Fe_2C_{98}H_{62}N_2O_{10}F_8$	$Fe_2C_{107.9}H_{84.7}N_2O_{12}F_8Cl_{1.1}$	$Fe_2C_{102}H_{70}N_2O_{12}F_8Cl_4$	$Fe_2C_{116}H_{108}O_{12}N_2$	$Fe_3C_{108}H_{88}O_{12}N_2Cl_4$
Formula weight	1691.20	1902.33	1921.10	1833.74	1915.15
Crystal System	Monoclinic	Monoclinic	Triclinic	Monoclinic	Orthorhombic
Space group	$P2_1/c$	$C2/c$	$P\bar{1}$	$P2_1/c$	$Pccn$
a (Å)	12.205(4)	23.578(5)	12.160(2)	16.035(3)	25.648(5)
b (Å)	24.088(7)	15.730(5)	13.918(3)	23.707(4)	14.847(3)
c (Å)	13.440(4)	25.052(6)	13.924(3)	13.007(2)	23.726(5)
α (deg)			105.674(3)		
β (deg)	97.980(6)	104.898(5)	92.481(3)	104.267(3)	
γ (deg)			106.665(3)		
V (Å^3)	3913(2)	8979(4)	2154.9(7)	4791.8(14)	9035(3)
Z	2	4	1	2	4
. ρ_{calc} (g/cm^3)	1.435	1.407	1.480	1.272	1.408
Temperature (K)	110	110	110	110	110
μ (Mo Kα), (mm^{-1})	0.456	0.438	0.545	0.368	0.660
Θ limits (deg)	2.28 to 25.68	2.12 to 27.12	2.18 to 25.03	2.16 - 25.68	2.20 – 27.10
Crystal size (mm)	0.08 × 0.10 × 0.20	0.10 × 0.10 × 0.15	0.10 × 0.15 × 0.10	0.06 × 0.22 × 0.40	0.06 × 0.20 × 0.35
Completeness to Θ	99.9 %	99.9 %	99.7 %	99.9 %	99.9 %
max, min peaks (e/Å^3)	0.691 and -0.678	0.680 and -0.940	0.946 and -0.578	1.381 and -0.737	0.458 and -0.373
Total no. of data	57171	72313	29990	69173	140867
No. of unique data	7431	9902	7661	9072	9962
Goodness-of-fit on F^2	1.112	1.104	1.121	1.030	1.089
R_1 (%)[a]	6.34	6.17	6.43	6.57	4.77
wR_2 (%)[b]	11.91	14.31	14.98	15.25	9.90

[a] $R1 = \Sigma||F_O|-|F_C||/\Sigma|F_O|$,

[b] $wR_2=\left\{\sum[w(F_o^2 - F_c^2)]/\sum[w(F_o^2)^2]\right\}^{1/2}$

Table 2

Selected Interatomic Bond Lengths (Å) and Angles (deg) for **1**–**4**.

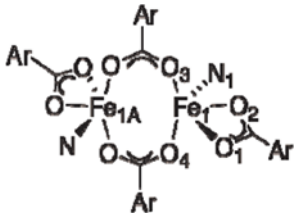

	1	**2**·1.5C_5H_{12}·0.5CH_2Cl_2	**3**·2CH_2Cl_2	**4**·2C_5H_{12}
Fe(1)–Fe(1A)	4.3679(16)	4.4243(9)	4.4153(12)	4.2743(12)
Fe(1)–N(1)	2.133(3)	2.132(2)	2.137(3)	2.137(3)
Fe(1)–O(1)	2.237(2)	2.308(2)	2.344(3)	2.398(3)
Fe(1)–O(2)	2.089(2)	2.0590(19)	2.054(2)	2.054(3)
Fe(1)–O(3)	1.967(2)	1.946(2)	1.955(3)	1.927(3)
Fe(1)–O(4)	2.018(2)	2.0182(19)	2.026(2)	2.028(3)
O(1)–Fe(1)–O(2)	60.33(8)	60.13(7)	59.56(9)	58.43(9)
O(1)–Fe(1)–O(3)	93.09(9)	95.87(8)	96.37(9)	104.65(10)
O(1)–Fe(1)–O(4)	101.00(9)	97.13(7)	97.60(9)	88.28(10)
O(2)–Fe(1)–O(3)	133.53(9)	131.98(9)	135.09(10)	134.04(12)
O(2)–Fe(1)–O(4)	109.52(10)	112.63(8)	110.45(10)	109.22(11)
O(3)–Fe(1)–O(4)	112.81(10)	111.12(9)	109.89(9)	112.74(12)
O(1)–Fe(1)–N(1)	153.88(9)	149.56(8)	154.56(9)	147.91(10)
O(2)–Fe(1)–N(1)	94.81(9)	89.46(9)	95.49(10)	90.10(11)
O(3)–Fe(1)–N(1)	99.97(10)	105.01(9)	99.40(10)	102.12(12)
O(4)–Fe(1)–N(1)	94.67(10)	95.71(8)	95.5(1)	97.45(11)
O(2)–O(5)	–	–	–	2.686(4)

Numbers in parentheses are estimated standard deviations of the last significant figures.

Table 3

Selected Bond Distances and Angles for **5**.

Bond Length (Å)			Bond Angle (deg)
Fe(1)–Fe(2)	3.4127(6)	Fe(1)–Fe(2)–Fe(1A)	133.98
Fe(1)–N(1)	2.1133(19)	Fe(1)–O(5)–Fe(2)	115.04(7)
Fe(1)–O(1)	2.0505(16)	O(4)–Fe(2)–O(4A)	104.85(9)
Fe(1)–O(2)	2.2931(17)	O(4)–Fe(2)–O(5)	113.00(6)
Fe(1)–O(3)	1.9715(16)	O(5A)–Fe(2)–O(4)	98.18(6)
Fe(1)–O(5A)	2.0596(16)	O(5)–Fe(2)–O(5A)	128.17(10)
Fe(2)–O(4)	2.0306(16)		
Fe(2)–O(5A)	1.9856(15)		

Numbers in parentheses are estimated standard deviations of the last significant figures.

Table 4

Mössbauer Parameters for a Solid Sample of **5**, Acquired at Different Temperatures.

Temperature (K)	δ (mm/s)	ΔE_Q (mm/s)	Γ (mm/s)
4.2	1.18(2)	2.92(2)	0.41
77	1.16(2)	2.88(2)	0.38
150	1.13(2)	2.76(2)	0.34
200	1.10(2)	2.67(2)	0.34